AIP | Applied Physics Letters

Resonant photoemission spectroscopy for intermediate band materials

F. Mazzola, M. Nematollahi, Z. S. Li, S. Cooil, X. Yang, T. W. Reenaas, and J. W. Wells

Citation: Applied Physics Letters **107**, 192104 (2015); doi: 10.1063/1.4935536
View online: http://dx.doi.org/10.1063/1.4935536
View Table of Contents: http://scitation.aip.org/content/aip/journal/apl/107/19?ver=pdfcov
Published by the AIP Publishing

Resonant photoemission spectroscopy for intermediate band materials

F. Mazzola,[1] M. Nematollahi,[1] Z. S. Li,[2] S. Cooil,[1] X. Yang,[1] T. W. Reenaas,[1] and J. W. Wells[1,a)]
[1]*Department of Physics, Norwegian University of Science and Technology (NTNU), NO-7491 Trondheim, Norway*
[2]*Department of Physics and Astronomy, Institute for Storage Ring Facilities, Aarhus (ISA), Ny Munkegade 120, Aarhus, DK-8000, Denmark*

(Received 26 June 2015; accepted 29 October 2015; published online 11 November 2015)

Resonant photoemission spectroscopy is used to study the intermediate-band material Cr doped ZnS. Using resonant photoemission, we show that the intermediate-band can be characterized, revealing the filling and specific orbital character of the states contributing to the resonant photoemission signal. We demonstrate that resonant photoemission spectroscopy is a powerful approach for understanding the origin of intermediate bands in doped ZnS. The methodology can be widely extended to a large variety of materials, providing useful information towards engineering of high efficiency intermediate band solar cells and of other optoelectronic devices. © *2015 AIP Publishing LLC*.
[http://dx.doi.org/10.1063/1.4935536]

Intermediate-band (IB) solar cells are devices consisting of a semiconductor with an electronic band within the material band-gap.[1,2] Such a band can be created, for example, by means of doping or by creating quantum dots in the host material.[3] IB-solar cells have attracted attention because of their high limiting-efficiency combined with a rather simple cell design.[4] Indeed, an efficiency limit[5] of 63% is predicted, cf. 41% for single gap solar cells, operating under the same conditions.[1] The increase in the efficiency arises because of the possibility of exciting electrons into the conduction band (CB) using multiple absorption processes.

In particular, in single gap solar cells, photons can excite electrons in the valence band (VB) and promote them into the CB; this mechanism can occur only if the energy of the excited electrons is at least the energy of the gap (E_g). In IB-solar cells not only the same mechanism can take place but also an additional 2-step process can occur. Indeed, since the IB forms within the band-gap, electrons of energy smaller than E_g can be first promoted into the IB, then from the IB can be excited into the CB. In other words, if the energy of the photons is not sufficient to promote an electron from the VB directly into the CB, the IB can be used as an additional stepping stone to generate electron-hole pairs.[6]

The combination of a high efficiency limit and a simple device design has resulted in an increasing interest in IB materials and IB-solar cells recently. A wide range of IB materials have been proposed and investigated, and characterization techniques for the device performance have been developed.[4] For detection of IB states within the bandgap, optical techniques such as photo- and electroluminescence,[7] photo-reflectance,[8] and spectroscopic ellipsometry[9] have been utilized, as well as electronic techniques such as deep level transient spectroscopy.[10] In general, a full characterization of the IB is crucial in order to control and eventually tune material properties to develop materials which are suitable for real devices.

In this work, we introduce an additional powerful approach based on resonant photoemission spectroscopy (RPES)[11] to access the nature of an IB. Even though this technique has been proven to be an efficient method to investigate several exotic phenomena in solid state materials,[12–17] it has not been used to characterize IB materials for photovoltaics. Specifically, we demonstrate that RPES is able to discriminate active and inactive orbital contribution of dopants, and directly probe the nature of the IB state, allowing for a quantification of the partial density of states (DOS) of such a band and the orbital character of the dopant species which give rise to it.

In this study, we use ≈4% Cr-doped ZnS as a model material,[18,19] but the same approach could be extended to a wide range of IB materials. The choice of ZnS as a test-material is related to the fact that its direct gap is quite large (3.6–3.9 eV), simplifying the detection of the Cr3d states responsible for the IB, forming within E_g. Moreover, ZnS is environmentally friendly, abundant, and is known to be a promising candidate for high-efficiency and non-toxic solar cells.[18–20]

The principle on which RPES is based is a quantum-mechanical interference between a direct photoemission process and a recombination of an excited state.[11] In Cr-doped ZnS, the direct photoemission process occurs from Cr valence electrons: photons excite an electron from the 3d energy level and bring it into the vacuum with kinetic energy E_K as in Fig. 1(a), $1s^2 2s^2 2p^6 3s^2 3p^6\ \mathbf{3d}^n 4s^1 + h\nu \rightarrow 1s^2 2s^2 2p^6 3s^2 3p^6 \mathbf{3d}^{(n-1)}\ 4s^1 + \mathbf{e}^-$, where n depends on the oxidation state of the Cr atom.

In such a material, the partially occupied 3d electronic DOS (e-DOS) of Cr is responsible for creating an IB within the energy gap of ZnS. To probe the existence of such a band we vary the photon energy ($h\nu$) across the Cr2p absorption edge; specifically we vary $h\nu$ from 570 eV to 590 eV. When the photon energy matches the transition Cr2p → Cr3d, electron transitions from the Cr2p into the Cr3d levels are possible. These electronic promotions can only occur for photon energies close to the Cr2p absorption edge[11] and are dictated

a)quantum.wells@gmail.com

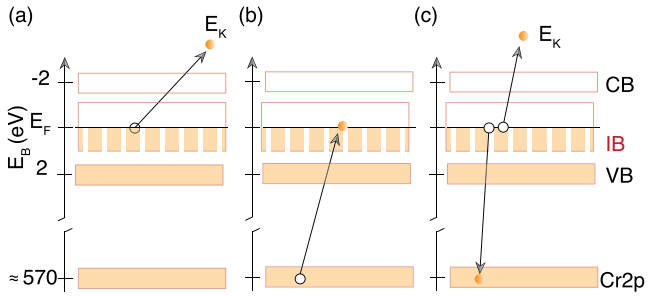

FIG. 1. Direct emission and resonant photoemission from the IB material; Cr doped ZnS. (a) Representation of the standard photoemission process: an electron is emitted from the IB (Cr3d in this illustration). (b) and (c) A secondary, 2-step, process: (b) the electron can be first excited from Cr2p into the Cr3d/IB state. (c) The Cr3d electron may then decay back to the Cr2p band by emission of another Cr3d electron. Both process ultimately lead to emission of a Cr3d electron and have the same initial and final states.

by the availability of unfilled (or partially filled) 3d orbitals and selection rules. In this recombination process, photons first promote a 2p electron into the 3d energy level, as illustrated in Fig. 1(b), then the extra electron in the 3d level decays back into the 2p level emitting a second electron with E_K, as in Fig. 1(c), $1s^2 2s^2 \mathbf{2p^6} 3s^2\ 3p^6 \mathbf{3d}^n 4s^1 + h\nu \rightarrow 1s^2 2s^2 \mathbf{2p^5}\ 3s^2 3p^6 \mathbf{3d}^{(n+1)}\ 4s^1 \rightarrow 1s^2 2s^2 \mathbf{2p}^6 3s^2 3p^6 \mathbf{3d}^{(n-1)}\ 4s^1 + \mathbf{e}^-$.

The final state of the direct photoemission and the recombination process is the same, or alternatively E_K of the emitted electron is the same. This results in a resonant enhancement of the intensity of the 3d states visible in the RPES spectra within the ZnS gap.

Since the resonant photoemission process involves modifying the occupancy of the 3d level by $\pm 1e^-$, it is a requirement that the 3d level is partially filled; otherwise, a resonant enhancement cannot occur. In the case of Cr doped ZnS, it is reasonable to assume a tetrahedral crystal field, which separates the 3d level into t_{2g} and e_g bands derived from (d_{xy}, d_{yz}, d_{xz}) and ($d_{x^2-y^2}$, d_{z^2}) orbitals, respectively.[18] t_{2g} and e_g may be partially filled and may show resonant behaviour. Since the energy of the Cr2p → Cr3d transition is dissimilar for Cr2p → t_{2g} and Cr2p → e_g, the photon energy required for resonance will be slightly different (as will the binding energy of the Cr3d t_{2g} and e_g states).

We performed the RPES experiment at MAT-line of the synchrotron radiation ASTRID2 and at D1011 beamline of MAX-II[21] under ultrahigh vacuum conditions ($P < 10^{-9}$ mbar) and at room temperature. ZnS samples with a nominal 4% Cr doping grown by both MBE and PLD were measured (see Ref. 9 for details of the sample growth). Both samples undergo cycles of sputtering in order to remove the native oxides at the surface, unavoidably formed after exposure of the samples to air. The core levels were monitored to ensure the absence of external contaminants in both samples. Oxygen was not completely removed for the MBE sample even after several sputtering cycles. We believe that this is due to the presence of oxygen at ZnS grain boundaries in this particular sample.

The RPES spectra from the MBE-sample are shown in Fig. 2(b) as a 2-dimensional (2D) image in false color scale (from white to blue, indicating from weak to strong intensity, respectively). Each column of the 2D image contains the intensity of the RPES spectra collected for a certain value of

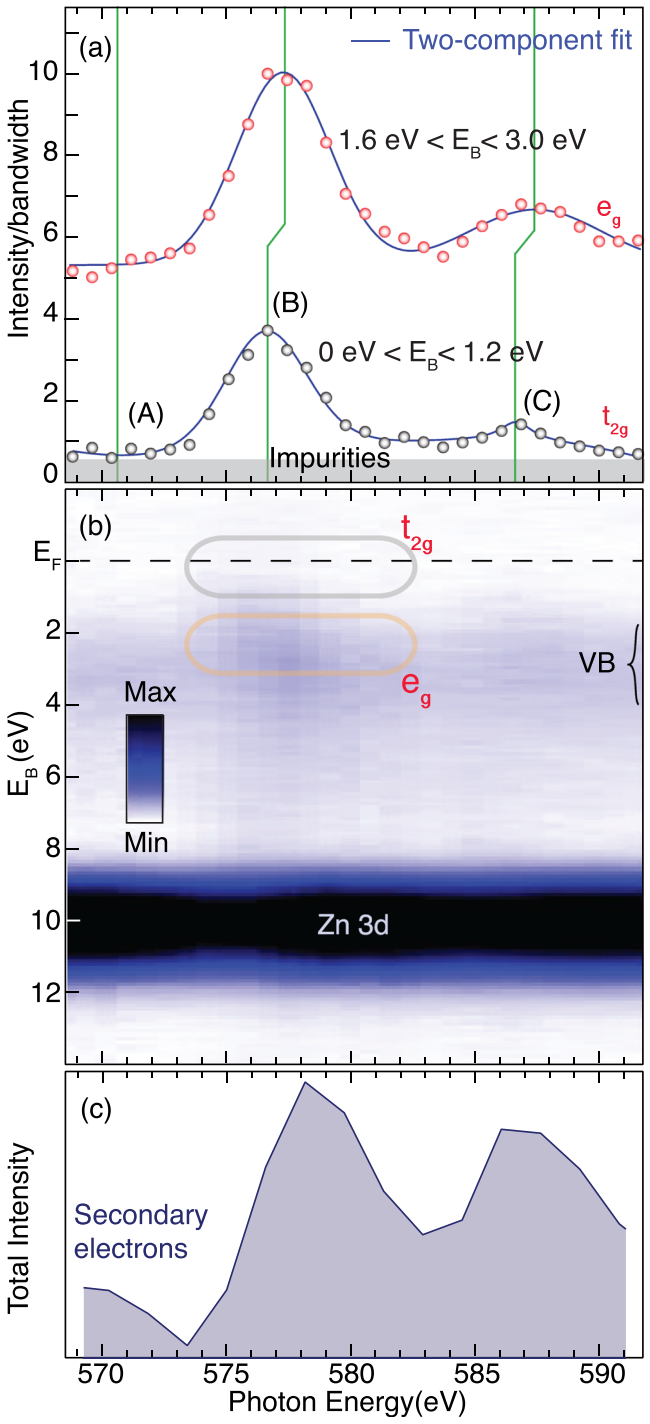

FIG. 2. RPES and XAS results. (a) Integrated RPES intensity in the range $E_B = 1.2$–0 eV (black markers) and $E_B = 3.0$–1.6 eV (red markers) normalized to the Zn3d core level and bandwidth. The markers are the experimental data and the blue lines are fit obtained by including only two components. The gray area is an approximate estimate of the impurity level in the sample. (b) 2D image plot in false color scale. Each column corresponds to one RPES spectrum and it is shown vs. photon energy. The resonant enhancements of the intensity close to the Fermi level and within the VB region and have been attributed to the orbital character Cr3d t_{2g} and e_g, respectively. (c) XAS measurements using partial electron yield. This measurement corresponds to the secondary electron emission from all processes.

photon energy. A typical RPES spectra, such as in Fig. 2(b), takes approximately 24 h of acquisition time. The same data are shown as an array of spectra in the supplementary material.[22] In Fig. 2(b), the most visible contributions within the E_B-range acquired are the Zn3d core level and the VB

maximum, falling at $E_B \approx 10\,\text{eV}$ and $E_B \approx 2\,\text{eV}$, respectively. Both Zn3d and VB are indicated in Fig. 2(b). When the photon energy matches the onset Cr2p → Cr3d, the resonant condition discussed above can occur and the 3d state will be visible within the ZnS gap because of the resonant enhancement of the Cr3d direct emission process. This means that when the resonant condition is fulfilled, there will be an increase in the intensity occurring within the ZnS gap, and this is directly observable in the 2D image plot. In other words, we can directly see the IB-DOS in the bandgap of ZnS. However, the Cr dopants constitute only 4% of the ZnS amount; thus, the IB intensity within the ZnS gap is weak.

In Fig. 2(b), resonances are visible and appear as broad intensity enhancements centered at photon energies around 577 and 587 eV. In order to make the resonant behaviour more clear, the photoemission intensity is extracted from Fig. 2(b) by integrating over two binding energy ranges, $E_B = 3.0$–$1.6\,\text{eV}$ and $E_B = 1.2$–$0\,\text{eV}$, depicted as the upper and lower traces of Fig. 2(a), respectively. Both of these regions show a resonant enhancement, but the photon energy of the resonant peak is shifted to higher photon energy for the larger binding energy resonance.

The two binding energy ranges chosen ($E_B = 3.0$–$1.6\,\text{eV}$ and $E_B = 1.2$–$0\,\text{eV}$) correspond to the e_g and t_{2g} binding energies, respectively, from which the photoemission signal is enhanced in RPES in the $\text{Cr2p} \rightarrow e_g$ and $\text{Cr2p} \rightarrow t_{2g}$ transitions (assuming a tetrahedral crystal field[18]). In both transitions, the Cr2p initial state is the same, but the *final* states (e_g and t_{2g}) differ in binding energy by $\approx 1.6\,\text{eV}$.

In both of the traces plotted in Fig. 2(a), two broad peaks (indicated by "B" and "C" in the figure) are visible. Such peaks originate from a similar excitation processes except that their *initial* states are different, i.e., $\text{Cr2p}_{1/2}$ and $\text{Cr2p}_{3/2}$. A two component fit of the data integrated over the energy range $E_B = 1.2$ and 0 eV yields a splitting of $9.7 \pm 0.2\,\text{eV}$, in good agreement with the expected spin-orbit splitting for $\text{Cr2p}_{1/2}$ and $\text{Cr2p}_{3/2}$.[23] The intensity of these two peaks could be expected to occur with a 1 : 2 ratio, reflecting the occupancy of the two initial states. However, the experimentally determined relative intensity is closer to 1:3. Such a difference can be attributed to the selection rules governing the transitions.[24,25] Whilst the relevant initial states are known, the momentum and spin of the available final states in a partially filled transition metal 3d band are less clear; however, unequal filling with respect to spin is expected for magnetic elements such as Cr. Hence, the possible transitions between the spin-orbit coupled $p_{1/2}$ and $p_{3/2}$ initial states, and the spin-orbit coupled and spin non-degenerate 3d final states will require that spin and orbital angular momentum conservation restrictions are satisfied. In short, the partial filling of the Cr3d t_{2g} derived IB imposes restrictions on the orbital character of the initial states from which excitations can occur, when examining this specific excitation channel. Such restrictions are indicative of a high-spin configuration and will have implications for the photo-excitations, which can occur in a photovoltaic, ultimately influencing device efficiency.

A quantitative estimate of the occupation of differing orbital character of the Cr e-DOS can be achieved by integrating the energy range within the ZnS gap and normalizing it to the Zn3d core level intensity to obtain the Cr3d t_{2g} contribution to the IB. From this and an estimate of the Cr3d e_g orbital character contribution to the VB, the identification of the Cr oxidation states can be made. If we integrate the intensity of the peaks in Fig. 2(a), we find that the intensity per unit bandwidth is very close to $e_g{:}t_{2g} = 2{:}1$. We therefore infer that e_g is half-filled (i.e., $2e^-$) and t_{2g} contains $1e^-$. This would be consistent with the Cr dopant being in the 2+ oxidation state with an electronic configuration $1s^2 2s^2 2p^6 3s^2 3p^6 3d^3 4s^1$. This also finds agreement with the observed 1:3 intensity ratio of transitions involving the $p_{1/2}$ and $p_{3/2}$ initial states, which implied a high-spin configuration of the IB and VB states, i.e., half-filled e_g and partially filled t_{2g} orbitals.

It is also interesting to observe that the total intensity of photoemission from the IB state is close to 3% of the Zn3d band, i.e., close to the nominal doping of the Cr doped ZnS sample. This indicates that ≈ 100% of the Cr dopants are contributing to the IB intensity. Since Cr is added in order to create the IB-DOS, any Cr present in the sample which is not contributing to it, corresponds to "wasted" Cr. One important aspect of photovoltaic material synthesis and characterisation is to understand and minimize such waste.

So far, we have focused on the dopant species contributing to the IB; however, the RPES analysis in Fig. 2(a) can also offer a quantitative estimate of the impurity concentration. Indeed, the constant offset in Fig. 2(a) is indicative of contributions to the DOS within the ZnS bandgap due to any element other than Cr. These contributions cannot be due to ZnS, since they are within the bulk bandgap, and they cannot be due to Cr because they do not resonate with the photon energy of the Cr edge. A precise quantification of this non-resonant DOS is challenging and we estimate it to be $\ll 1\%$ with respect to the Zn amount.

We have conducted highly complementary X-ray absorption spectroscopy (XAS) measurements on the same sample and with the same experimental setup used for RPES, but in this case, it is the low kinetic energy secondary electrons which are collected. The XAS results have been carefully calibrated and are summarized in Fig. 2(c). Whilst the RPES intensity at the Fermi level contains information on the Cr orbitals which are actively contributing to the IB-DOS, XAS contains information on the total amount of the Cr present. The XAS peaks appear at higher photon energy than the RPES peaks, indicating that there is a higher energy Cr transition contributing to the XAS signal. This could be due, for example, to a small quantity of Cr_2O_3, which we believe to be present at grain boundaries, but which does not contribute to the IB-DOS. For high Cr concentrations, it is possible that metallic Cr clusters form, although not observable in our experimental data.

XAS measurements with partial yield are also important to rule out the possibility of a contribution to the RPES intensities from the second order light generated by the beamline. Indeed, in synchrotron experiments, for each excitation energy used $h\nu$, a small amount of second order light (with energy $2h\nu$) can be generated too (for MAT-line, this contribution is expected to be very small in this energy range). In principle, the second order light could give rise to additional core-level transitions, which would obfuscate the RPES data (but not the XAS data). The similarity of the

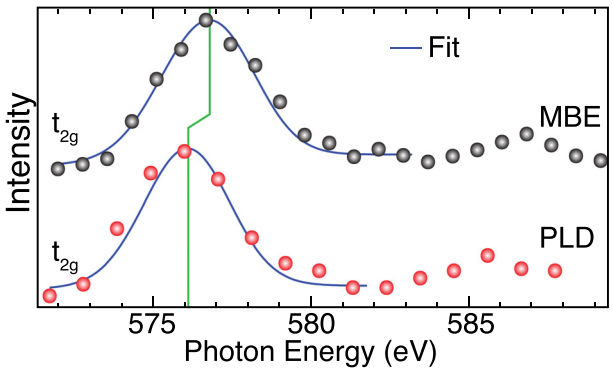

FIG. 3. Comparison of nominally identical samples grown by using MBE and PLD. The partial DOS is obtained by integrating the intensities in the range $E_B = 1.2$–0 eV. The blue line is the fitted peak position. The vertical green line indicates the maxima of the fit for the two samples.

XAS and RPES data confirms the detected features derive from the first order light. This is not surprising, given the low flux of $2h\nu$ expected at these energies. The second order photoemission would also give rise to linearly dispersing features in the RPES image in Fig. 2(b), and no such artefacts are observed.

To further illustrate the potential of the RPES method, we have investigated a nominally identical Cr doped ZnS sample grown by an alternative growth method, PLD. The results have been summarized in Fig. 3. The data have been both carefully calibrated for the photon energies used. Moreover, the nominal doping of the two samples is the same, which is also confirmed by the integrated RPES intensity, but subtle differences are also revealed. For the PLD sample, the intensity per unit bandwidth (integrated over the same limits as for the MBE sample) is $e_g{:}t_{2g} \approx 2{:}1.5$, indicating a slightly increased filling of the t_{2g} orbital (compared to the MBE sample). We infer that, whilst the MBE sample mainly contains Cr^{2+} with electronic configuration $1s^2 2s^2 2p^6 3s^2 3p^6 3d^3 4s^1$, the PLD sample contains relatively more Cr^{+} with an increased occupancy of the 3d t_{2g} orbital. In any case, RPES allows subtle differences in the IB band to be seen for nominally identical samples.

In conclusion, we have demonstrated the applicability of RPES in studying IB materials relevant to photovoltaics. RPES is not only able to reveal quantitative information on the partial DOS within the material bandgap but also able to reveal the origin of these states and their orbital character. In the present case, we demonstrate the contribution of Cr orbitals in Cr doped ZnS, and are able to compare two similar samples prepared using different growth methods. In addition, we have performed XAS measurements, which facilitates an understanding of the total amount of each species present in the sample. Thus, the powerful combination of RPES and XAS allows us to understand the orbitals which actively contribute to the intermediate band. Such characterization of IB materials is important in the development of materials for high efficiency photovoltaics. Whilst we have concentrated on Cr doped ZnS, it is important to point out that this approach of combining XAS and RPES is of much broader relevance and can be applied to a large variety of IB materials such as complex oxides and quantum dots solar cells, which have much potential as next generation photovoltaic devices.

Dr. A. Preobrajenski of beamline D1011 at the MAX IV Laboratory is gratefully acknowledged for his assistance and insightful discussions. This work was supported in part by The Norwegian Center for Solar Cell Technology, a Center for Environment-Friendly Energy Research co-sponsored by the Norwegian Research Council and Research and Industry in Norway (Project No. 193829). The authors also acknowledge the Research Council of Norway for financial support via the Nano2021 program (Project No. 203503).

[1]A. Luque and A. Martí, Phys. Rev. Lett. **78**, 5014 (1997).
[2]Y. Okada *et al.*, "Intermediate band solar cells: Recent progress and future directions," Appl. Phys. Rev. **2**, 021302 (2015).
[3]T. Sogabe, Y. Shoji, M. Ohba, K. Yoshida, R. Tamaki, H.-F. Hong, C.-H. Wu, C.-T. Kuo, S. Tomić, and Y. Okada, Sci. Rep. **4**, 4792 (2014).
[4]I. Ramiro, A. Marti, E. Antolin, and A. Luque, IEEE J. Photovoltaics **4**, 736 (2014).
[5]W. Shockley and H. J. Queisser, J. Appl. Phys. **32**, 510 (1961).
[6]A. Luque, A. Marti, and C. Stanley, Nat. Photonics **6**, 146 (2012).
[7]A. Luque, A. Martí, N. López, E. Antolín, E. Cánovas, C. Stanley, C. Farmer, L. J. Caballero, L. Cuadra, and J. L. Balenzategui, Appl. Phys. Lett. **87**, 083505 (2005).
[8]K. M. Yu, W. Walukiewicz, J. Wu, W. Shan, M. A. Scarpulla, O. D. Dubon, J. W. Beeman, and P. Becla, Phys. Status Solidi B **241**, 660 (2004).
[9]M. Nematollahi, X. Yang, L. M. S. Ass, Z. Ghadyani, M. Kildemo, U. Gibson, and T. W. Reenaas, "Molecular beam and pulsed laser deposition of ZnS:Cr for intermediate band solar cells," Sol. Energy Mater. Sol. Cells **141**, 322–330 (2015).
[10]M. Ichimura, H. Sakakibara, K. Wada, and M. Kato, J. Appl. Phys. **114**, 114505 (2013).
[11]C. Guillot, Y. Ballu, J. Paigné, J. Lecante, K. P. Jain, P. Thiry, R. Pinchaux, Y. Pétroff, and L. M. Falicov, Phys. Rev. Lett. **39**, 1632 (1977).
[12]H. Sato, M. Koyama, K. Takada, H. Okuda, K. Shimada, Y. Ueda, J. Ghijsen, and M. Taniguchi, J. Electron Spectrosc. Relat. Phenom. **88**, 333–337 (1998).
[13]M. Weinelt, A. Nilsson, M. Magnuson, T. Wiell, N. Wassdahl, O. Karis, A. Föhlisch, N. Mårtensson, J. Stöhr, and M. Samant, Phys. Rev. Lett. **78**, 967 (1997).
[14]F. Mazzola, M. T. Edmonds, K. Høydalsvik, D. J. Carter, N. A. Marks, B. C. C. Cowie, L. Thomsen, J. Miwa, M. Y. Simmons, and J. W. Wells, ACS Nano **8**, 10223 (2014).
[15]P. Hofmann, C. Søndergaard, S. Agergaard, S. V. Hoffmann, J. E. Gayone, G. Zampieri, S. Lizzit, and A. Baraldi, Phys. Rev. B **66**, 245422 (2002).
[16]L. C. Davis, Phys. Rev. B **25**, 2912 (1982).
[17]L. Bawden, J. M. Riley, C. H. Kim, R. Sankar, E. J. Monkman, D. E. Shai, H. I. Wei, E. Lochocki, J. W. Wells, W. Meevasana, T. K. Kim, M. Hoesch, Y. Ohtsubo, P. Le F'evre, C. J. Fennie, K. M. Shen, F. C. Chou, and P. D. C. King, Sci. Adv. **1**(8), e1500495 (2015).
[18]C. Tablero, Phys. Rev. B **74**, 195203 (2006).
[19]C. Tablero, J. Chem. Phys. **123**, 114709 (2005).
[20]J. Schrier, D. O. Demchenko, Lin-Wang, and A. P., Alivisatos, "Optical properties of ZnO/ZnS and ZnO/ZnTe heterostructures for photovoltaic applications," Nano Lett. **7**(8), 2377–2382 (2007).
[21]R. Nyholm, S. Svensson, J. Nordgren, and A. Flodström, Nucl. Instrum. Methods Phys. Res., Sect. A **246**, 267 (1986).
[22]See supplementary material at http://dx.doi.org/10.1063/1.4935536 for an alternative presentation of the raw data.
[23]J. C. Fuggle and N. Mårtensson, J. Electron Spectrosc. Relat. Phenom. **21**, 275 (1980).
[24]A. S. Vinogradov, S. I. Fedoseenko, S. A. Krasnikov, A. B. Preobrajenski, V. N. Sivkov, D. V. Vyalikh, S. L. Molodtsov, V. K. Adamchuk, C. Laubschat, and G. Kaindl, Phys. Rev. B **71**, 045127 (2005).
[25]P. Olalde-Velasco, J. Jiménez-Mier, J. D. Denlinger, Z. Hussain, and W. L. Yang, Phys. Rev. B **83**, 241102 (2011).